



HAL
open science

Turbulent heat transfer predictions using the v2-f model on unstructured meshes

Remi Manceau, S. Parneix, D. Laurence

► To cite this version:

Remi Manceau, S. Parneix, D. Laurence. Turbulent heat transfer predictions using the v2-f model on unstructured meshes. *International Journal of Heat and Fluid Flow*, 2000, 21 (3), pp.320-328. 10.1016/S0142-727X(00)00016-3 . hal-02991043

HAL Id: hal-02991043

<https://hal.science/hal-02991043>

Submitted on 5 Nov 2020

HAL is a multi-disciplinary open access archive for the deposit and dissemination of scientific research documents, whether they are published or not. The documents may come from teaching and research institutions in France or abroad, or from public or private research centers.

L'archive ouverte pluridisciplinaire **HAL**, est destinée au dépôt et à la diffusion de documents scientifiques de niveau recherche, publiés ou non, émanant des établissements d'enseignement et de recherche français ou étrangers, des laboratoires publics ou privés.



Distributed under a Creative Commons Attribution - NonCommercial - NoDerivatives 4.0
International License

Turbulent heat transfer predictions using the $\overline{v^2-f}$ model on unstructured meshes

R. Manceau^{a,*}, S. Parneix^{a,1}, D. Laurence^{a,b}

^a*Mécanique des fluides et transferts thermiques, Électricité de France, 6 quai Watier, BP 49, 78 401 Chatou, France*

^b*Department of Mechanical Engineering, UMIST, George Begg Building, Sackville Street, Manchester, M60 1QD, UK*

^{*}*Corresponding author: Heat Transfer Section, Faculty of Applied Physics, TU Delft, Lorentzweg 1, 2628 CJ Delft, the Netherlands*
E-mail: manceau@ws.tn.tudelft.nl; Tel: +31 (0)15 278 6157; Fax: +31 (0)15 278 1204

¹*Present address: Heat Transfer, ABB ALSTOM Power Technology Ltd., CH-5405 Baden-Dättwil, Switzerland*

Abstract

Durbin's three transport equation model, the so-called $\overline{v^2-f}$ model, has been implemented in an industrial finite element code, N3S, developed at the research and development department of Électricité de France, enabling the use of unstructured meshes. Validations by comparison with other codes have been performed in the cases of the channel flow at $Re_\tau = 395$, and the backward-facing step at $Re = 5, 100$. The test case of the 2D periodic ribbed-channel flow has then been computed, without heat transfer at $Re_H = 37, 200$, and with a constant heat flux imposed at the ribbed-wall at $Re_H = 12, 600$. The results obtained show the ability of the model to predict accurately the enhancement of heat transfer due to the ribs, which is of primary interest for industrial applications.

Keywords: $\overline{v^2-f}$ model; low-Reynolds number; heat transfer; unstructured mesh; backstep; ribbed channel.

Notation

D_e	Hydraulic diameter	U_b	Bulk velocity
D_{ij}^T	Turbulent diffusion tensor	u_τ	Friction velocity
e	Rib height	$\overline{v^2}$	Scalar velocity scale of the $\overline{v^2}$ - f model
f	Variable related to energy redistribution in the equation of the scalar velocity scale $\overline{v^2}$		
			<i>Greek</i>
		α	Thermal diffusivity
		Δt	Time step
h	Characteristic length scale of the flow	ε	Turbulent kinetic energy dissipation rate
k	Turbulent kinetic energy	ε_{ij}	Dissipation tensor
L	Length scale used in the $\overline{v^2}$ - f model	λ	Thermal conductivity
\mathbf{n}	Unit vector normal to the wall	ν	Molecular cinematic viscosity
Nu	Nusselt number	ν_T	Eddy viscosity
Nu_s	Nusselt number for the turbulent flow in a smooth circular pipe	$\nu_{T_{lm}}$	Generalised eddy viscosity
		θ	Fluctuating temperature
p	Mean pressure	Θ	Mean temperature
P	Production of turbulent kinetic energy	ϕ_{ij}^h	Homogeneous model for the redistribution term
Pr	Prandtl number		
Pr_T	Turbulent Prandtl number		
\dot{q}	Heat flux		
Re_H	Reynolds number $U_b D_e / \nu$		
Re_τ	Reynolds number $u_\tau h / \nu$		
Re	Reynolds number $U_b h / \nu$		
s	curvilinear coordinate		
S_{ij}	Deformation rate tensor		
T	Time scale used in the $\overline{v^2}$ - f model	(n)	Value of the variable at the n^{th} time step
			<i>Superscripts</i>

	<i>Subscripts</i>		
b	Bulk value	$\bar{\varphi}$	Ensemble mean of a variable φ
n	Wall-normal component	$\tilde{\varphi}$	Convected value of a variable φ
w	Wall value	D/Dt	Substantial derivative
	<i>Operators</i>		

1 Introduction

In industrial applications of computational fluid dynamics, turbulence models have been so far generally restricted to high-Reynolds number regions, and the wall vicinity accounted for by wall functions. However, the latter are based on the assumption that the near-wall flow satisfies a universal behaviour, which is not the case in most of the applications of industrial interest, such as flows with low-Reynolds, separation or impingement regions. In particular, this approach is not suitable to heat transfer calculations in nuclear engineering. Therefore, models integrable down to solid boundaries are needed.

Low-Reynolds models are generally derived from high-Reynolds models by introducing damping functions or extra nonlinear terms to account for the effect of the wall on turbulence (i.e. Craft *et al.*, 1996; Iacovides and Raisee, 1999). However, such methods are rather *ad hoc*, since the high-Reynolds-number models are based on the assumptions that the variations of the velocity gradient can be neglected in the rapid part of the redistribution term (quasi-homogeneity) and that terms involving the pressure can be modelled by algebraic expressions (locality): both assumptions are not valid in the wall region (Manceau, 1999). In particular, the kinematic effects of the wall, such as the blocking of the normal fluctuating velocity component, are fundamentally non-local, and cannot be properly reproduced by an algebraic model without introducing an explicit dependence on the wall-distance. This is at the origin of the success of the so-called *wall-echo terms*. Unfortunately, such terms are ill-behaved in general geometries and are therefore not suitable to industrial cases.

The elliptic relaxation method (Durbin, 1991) allows the derivation of wall-proximity models which does not suffer from the previously emphasized shortcomings: the quasi-homogeneous assumption is not used and the redistributive term is given by a differential equation, the so-called *elliptic relaxation equation*, which enables the reproduction of the non-local effect. Moreover, this method is related to a theoretical analysis, which proved to be consistent with DNS data (Manceau *et al.*, 2000).

The $\overline{v^2}$ - f model is an elliptic relaxation model reduced to three transport equations. It is based on a turbulent viscosity hypothesis, but contains and uses information on the anisotropy of the flow in the near-wall region through the evaluation of the turbulent scale $\overline{v^2}$, which is locally similar to the normal Reynolds stress $\overline{u_n^2}$ in the vicinity of the wall. In the frame of industrial applications, this model represents a good compromise between two-equation models, which are widely used for their simplicity and robustness, and full Reynolds stress models, closer to the physics, but very stiff

numerically. Moreover, the $\overline{v^2}$ - f model has been successfully applied in many complex situations (Durbin, 1995; Parneix *et al.*, 1998a; Parneix *et al.*, 1998b; Lien *et al.*, 1997; Behnia *et al.*, 1998; Behnia *et al.*, 1999). This model has thus been selected for use in the industrial code N3S, developed at EDF, for its ability to reproduce accurately the near-wall turbulence and to predict heat transfer.

The distinctive feature of this work is the use of unstructured meshes: all previous $\overline{v^2}$ - f computations used structured meshes. The first section of the paper describes briefly the $\overline{v^2}$ - f model. More details, and in particular the justification of the model, are given by Durbin (1991) or Manceau (1999). The second section presents the implementation of the model in the finite element code N3S and in particular how the boundary conditions are handled, as well as the validation which has been conducted for the cases of the channel and backstep flows. The third section is devoted to the test case of a 2D periodic ribbed-channel, which is relevant for turbine cooling. Two sets of experiments are available for this case: the first one, with flow measurements, from Drain and Martin (1985), at $Re_H = 37,200$; the second one, with heat flux measurements on the ribbed-wall, from Liou *et al.* (1993), at $Re_H = 12,600$. Both cases were computed separately and the influence of the temperature boundary conditions for the second case has been investigated.

2 The V2F model

High-Reynolds-number turbulent viscosity models need strong corrections to be applicable down to solid boundaries. The $\overline{v^2}$ - f model is explicitly derived in order to avoid the use of *ad hoc* damping functions. In particular, the function f_μ , which corrects the strong overestimation of the turbulent viscosity in the vicinity of the wall and, consequently, of the shear stress \overline{uv} , is not needed.

In this purpose, Durbin (1991) suggested to use the following expression for the turbulent viscosity close to a solid boundary, 2 being the direction normal to the wall:

$$\nu_T = C_\mu \overline{u_2 u_2} T \tag{1}$$

with $T = k/\varepsilon$. This expression is similar to the standard Prantl–Kolmogorov formula, in which k is replaced by $\overline{u_2 u_2}$, which provides the expected damping of the turbulent viscosity (e.g. Launder, 1988).

However, the Reynolds stresses are not calculated in a two-equation model. Since the evaluation of $\overline{u_2 u_2}$ by the Boussinesq equation is obviously not possible in this case, Durbin proposed to solve a transport equation for a scalar

velocity scale (called “ $\overline{v^2}$ ”), directly derived from the transport equation of the wall-normal Reynolds stress $\overline{u_2 u_2}$ in a channel:

$$\frac{D\overline{u_2 u_2}}{Dt} = k f_{22} - \frac{\overline{u_2 u_2}}{k} \varepsilon + \nabla \cdot ((\nu + \nu_T) \nabla \overline{u_2 u_2}) \quad (2)$$

where the term $k f_{22}$ stands for the redistributive term. In order to preserve the non-local effect in this equation, f_{22} is modelled by the following elliptic relaxation equation:

$$f_{22} - L^2 \nabla^2 f_{22} = \frac{1}{k} \phi_{22}^h \quad (3)$$

in which the slow and rapid parts of the source term ϕ_{22}^h are respectively given by Rotta and IP models (Naot *et al.*, 1973).

The dissipation term ε_{22} has been split into two parts: $\varepsilon \overline{u_2 u_2}/k$ and $\varepsilon_{22} - \varepsilon \overline{u_2 u_2}/k$. The second one is also assumed to follow an elliptic relaxation equation and is thus included in the term $k f_{22}$. Hence, the homogeneous source term $(\varepsilon \overline{u_2 u_2}/k - 2/3 \varepsilon)/k$ is added in Eq. (3):

$$f_{22} - L^2 \nabla^2 f_{22} = \frac{1}{k} \left(\phi_{22}^h + \frac{\overline{u_2 u_2}}{k} \varepsilon - \frac{2}{3} \varepsilon \right) \quad (4)$$

Since $k f_{22}$ goes to zero at the wall, the total dissipation ε_{22} is $\varepsilon \overline{u_2 u_2}/k$ in the near-wall region and tends to its isotropic value $\frac{2}{3} \varepsilon$ far from the wall.

The use of the elliptic equation (4) allows the integration of the model down to solid boundaries, since $\overline{u_2 u_2}$ and thus the eddy-viscosity is correctly damped, when the appropriate boundary condition for f_{22} is provided (Durbin, 1991):

$$f_{22} = -\frac{20 \nu^2 \overline{u_2 u_2}}{\varepsilon x_2^4} \quad (5)$$

In the model, called $\overline{v^2}$ - f , $\overline{u_2 u_2}$ and f_{22} are replaced by scalars denoted $\overline{v^2}$ and f in equations (2) and (4), which are solved in addition to equations for k and ε . $\overline{v^2}$ is then no longer comparable to the corresponding Reynolds stress component $\overline{u_2 u_2}$, but must be considered as a scalar velocity scale, tending to $\overline{u_n u_n}$ near any solid wall, n being the normal direction to this wall, thus providing an estimation of the turbulence anisotropy near all solid boundaries. Equations (2) and (4) has been derived from the equations of $\overline{u_2 u_2}$ and f_{22} in a channel, but are applicable in arbitrary geometries.

The model consists in the following equations:

- Equations:

$$\frac{DU}{Dt} = -\nabla p + \nabla \cdot ((\nu + \nu_T)(\nabla U + \nabla^t U)) \quad (6)$$

$$\frac{Dk}{Dt} = P - \varepsilon + \nabla \cdot ((\nu + \nu_T)\nabla k) \quad (7)$$

$$\frac{D\varepsilon}{Dt} = \frac{C'_{\varepsilon_1}P - C_{\varepsilon_2}\varepsilon}{T} + \nabla \cdot \left((\nu + \frac{\nu_T}{\sigma_\varepsilon})\nabla \varepsilon \right) \quad (8)$$

$$\frac{D\overline{v^2}}{Dt} = k f - \frac{\overline{v^2}}{k}\varepsilon + \nabla \cdot ((\nu + \nu_T)\nabla \overline{v^2}) \quad (9)$$

$$f - L^2\nabla^2 f = (C_1 - 1)\frac{(2/3 - \overline{v^2}/k)}{T} + C_2\frac{P}{k} \quad (10)$$

$$\nu_T = C_\mu\overline{v^2}T \quad ; \quad P = 2\nu_T S_{ij}S_{ij} \quad (11)$$

- Length and time scales:

$$L = C_L \max \left(\frac{k^{3/2}}{\varepsilon} ; C_\eta \left(\frac{\nu^3}{\varepsilon} \right)^{1/4} \right) ; \quad T = \max \left(\frac{k}{\varepsilon} ; 6 \left(\frac{\nu}{\varepsilon} \right)^{1/2} \right) \quad (12)$$

- Coefficients: $C'_{\varepsilon_1} = 1.4 \left(1 + 0.045(k/\overline{v^2})^{1/2} \right)$

$$\begin{aligned} C_\mu &= 0.22 ; C_1 = 1.4 ; C_2 = 0.3 ; C_{\varepsilon_2} = 1.9 ; \\ \sigma_\varepsilon &= 1.3 ; C_L = 0.25 ; C_\eta = 85.0 \end{aligned} \quad (13)$$

- Boundary conditions at walls:

$$U_i = 0 ; k = 0 ; \overline{v^2} = 0 ; \varepsilon = \frac{2\nu k}{y^2} ; f = -\frac{20 \nu^2 \overline{v^2}}{\varepsilon y^4} \quad (14)$$

- Realisability constraints:

$$T \leq \frac{0.6k}{6^{1/2}C_\mu\overline{v^2}S_{ij}S_{ij}} ; \quad L \leq C_L \frac{k^{3/2}}{6^{1/2}C_\mu\overline{v^2}S_{ij}S_{ij}} \quad (15)$$

These equations are based on the standard k - ε equations and only some comments are needed: the time and length scales are bounded by Kolmogorov scales in order to suppress singularities in the ε and f equations, respectively; a variable coefficient C'_{ε_1} has been introduced in order to enhance the generation of ε at the wall (it goes to infinity as y^{-2} in the vicinity of the wall but since P behaves as y^4 in this model, the product $C'_{\varepsilon_1}P$ goes to zero, so no unstability problem were expected and have been encountered); the source term of the f equation is exactly derived from (4), replacing ϕ_{22}^h by the Rotta+IP model; the coefficients of the model are those used by Parneix *et al.* (1998b).

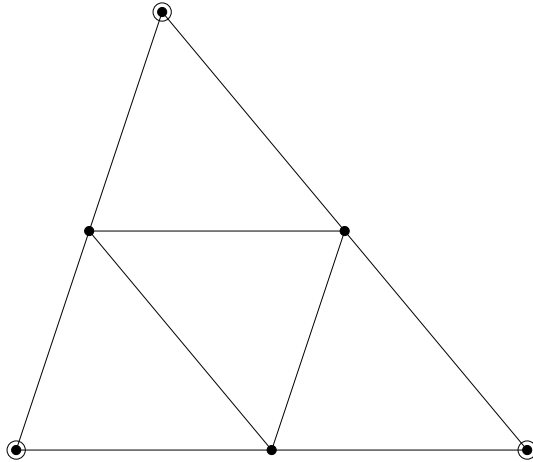


Figure 1: P1–isoP2 element divided into four sub-elements. \circ pressure nodes; \bullet velocity nodes.

3 Implementation and validation

3.1 The N3S code

N3S is an industrial code developed at the research and development department of EDF. It uses finite elements, which are triangles in 2D and tetrahedra in 3D. The discretization is P1–isoP2: the pressure is evaluated at the nodes of the element (P1 nodes) and for all other variables, discretization points are added at the middle of each edge (P2 nodes). For instance, in 2D cases, there are three P1 nodes and six P2 nodes per element, as shown in Fig. 1.

The terminology *iso* means that the P2 variables are not projected on quadratic but linear basis functions: in 2D, by adding nodes at the middle of the edges, four sub-elements are defined, in which linear basis functions are used. P1–isoP2 elements have the advantage of satisfying the *inf-sup* condition.

The time discretization is based on a fractional step method. The first step is the convection step, resolved by the characteristic method with a fourth order Runge–Kutta algorithm. The second step is the diffusion of all scalar variables. The third and last one is the resolution of the generalized Stokes problem (velocity–pressure system) by either a Chorin or a Uzawa algorithm. More details about the method used in the code can be found in Chabard *et al.* (1996). Only the points peculiar to the $\overline{v^2}$ – f model will be described.

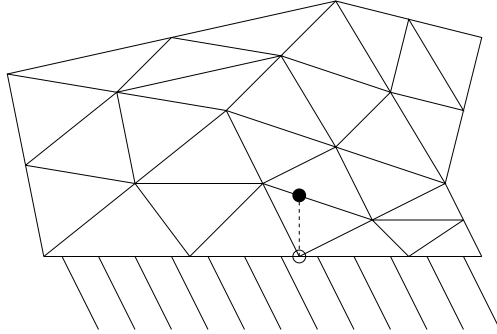


Figure 2: Method used for the evaluation of the limiting values involved in the wall boundary conditions. \circ point where the boundary conditions $\varepsilon = 2\nu k/y^2$ and $f = -20\nu^2\overline{v^2}/\varepsilon y^4$ are applied; \bullet point where the limiting values k/y^2 and $\overline{v^2}/y^4$ are evaluated.

3.2 Boundary conditions

The method to be used for the resolution of the turbulence equations is mainly imposed by the boundary conditions of the model. Indeed, whereas the conditions $k = 0$ and $\overline{v^2} = 0$ are simply accounted for by a projection method, those on ε and f require the solving of a coupled system for k and ε on one hand, and for $\overline{v^2}$ and f on the other hand.

The wall boundary conditions on $\overline{v^2}$ and f involve the limiting values $\lim_{y \rightarrow 0} k/y^2$ and $\lim_{y \rightarrow 0} \overline{v^2}/y^4$, respectively. With a Cartesian grid, these values can be simply evaluated at the first node inside the domain. With triangular finite elements (only 2D cases are considered herein), this method is not directly applicable, since no other node of the element is generally located in the wall-normal direction. However, as shown on Fig. 2, the limiting values can be evaluated by interpolation at the point where the first edge of the mesh is encountered in the normal direction. This simple method, similar to a finite difference method, has been totally satisfactory.

The boundary conditions on ε and f thus involve the values of k and $\overline{v^2}$, respectively, in the two points inside the domain defining the first encountered edge. The simplest solution would be to account for this coupling in an explicit manner. Unfortunately, this method can lead to numerical instabilities: the ratios k/y^2 and $\overline{v^2}/y^4$ can take large values when k and $\overline{v^2}$ deviate from their asymptotic behaviour in y^2 and y^4 , respectively. Therefore, it has been found necessary to couple implicitly the k and ε equations on one hand, and the $\overline{v^2}$ and f equations on the other.

3.3 Resolution of the coupled systems

Two coupled systems k - ε and $\overline{v^2}$ - f are thus to be solved. With the convection being accounted for by the method of characteristics, the substantial derivatives in the transport equations of these four variables can be recast as

$$\frac{D\varphi}{Dt} = \frac{\varphi^{(n+1)} - \tilde{\varphi}^{(n)}}{\Delta t} \quad (16)$$

where φ is any of the variables, the bracketed exponent indicates the iteration number, Δt the time step and $\tilde{\varphi}^{(n)}$ the convected value of $\varphi^{(n)}$.

In the resolution of the systems k - ε and $\overline{v^2}$ - f , the coupling enables the implicitation of terms which are usually taken explicit, such as ε in the k equation and f in the $\overline{v^2}$ equation. The method can be summarized as

$$\begin{cases} \frac{k^{(n+1)} - \tilde{k}^{(n)}}{\Delta t} = P^{(n)} - \varepsilon^{(n+1)} + \nabla \cdot \left((\nu + \nu_T^{(n)}) \nabla k^{(n+1)} \right) \\ \frac{\varepsilon^{(n+1)} - \tilde{\varepsilon}^{(n)}}{\Delta t} = \frac{C'_{\varepsilon_1} P^{(n)} - C_{\varepsilon_2} \varepsilon^{(n+1)}}{T^{(n)}} + \nabla \cdot \left(\left(\nu + \frac{\nu_T^{(n)}}{\sigma_\varepsilon} \right) \nabla \varepsilon^{(n+1)} \right) \end{cases} \quad (17)$$

$$\begin{cases} \frac{\overline{v^2}^{(n+1)} - \tilde{\overline{v^2}}^{(n)}}{\Delta t} = k^{(n)} f^{(n+1)} - \frac{\overline{v^2}^{(n+1)}}{k^{(n)}} \varepsilon^{(n)} + \nabla \cdot \left((\nu + \nu_T^{(n)}) \nabla \overline{v^2}^{(n+1)} \right) \\ f^{(n+1)} - L^{(n)2} \nabla^2 f^{(n+1)} = (C_1 - 1) \frac{(2/3 - \overline{v^2}^{(n)}/k^{(n)})}{T^{(n)}} + C_2 \frac{P^{(n)}}{k^{(n)}} \end{cases} \quad (18)$$

The boundary conditions for ε and f are taken implicit:

$$\varepsilon^{(n+1)} = 2\nu \frac{k^{(n+1)}}{y^2} \quad (19)$$

and

$$f^{(n+1)} = -\frac{20\nu^2 \overline{v^2}^{(n+1)}}{\varepsilon^{(n)} y^4} \quad (20)$$

and are evaluated as described in Fig. 2. These boundary conditions are directly imposed in the matrices of the systems whose solutions are obtained by a BI-CGSTAB algorithm (Van der Worst, 1992).

3.4 Validation

3.4.1 Channel flow

In order to validate the implementation of the $\overline{v^2}$ - f model, the results given by N3S have been compared to those given by a 1D code developed at the

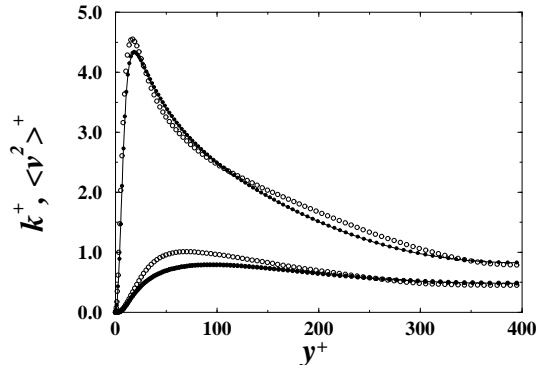


Figure 3: Validation of the implementation in N3S. Channel flow at $Re_\tau = 395$. k and $\overline{v^2}$ profiles. \bullet 1D code; — N3S; \circ DNS.

Center for Turbulence Research, in Stanford University. The case of the channel flow at $Re_\tau = 395$ has been chosen, and the results can be thus compared with the DNS (Moser *et al.*, 1999).

The problem is resolved on a 2D periodic domain, with only three nodes in the direction of the flow. The mesh is made of triangles obtained by dividing rectangles by one of their diagonals. The mesh has been intentionally chosen very fine in the y -direction, in order to ensure that the discretization error is negligible. The first point inside the domain is located at $y^+ = 0.5$ and the mesh contains 200 velocity nodes in the half-height of the channel. A symmetry boundary condition is applied at the centre.

The results obtained for k and $\overline{v^2}$ are shown in Fig. 3. A perfect coincidence between the profiles given by N3S and the 1D code is observed. This validates the implementation and in particular the way the boundary conditions are handled. It can also be seen that the results are in good agreement with the DNS data. Note that the $\overline{v^2}$ - f model is able to reproduce naturally the fluctuations of normal velocity, thus providing the right scaling for turbulent transport near the wall without any *ad-hoc* damping functions.

3.4.2 Backward-facing step

The second test case that has been chosen in order to validate the implementation of the $\overline{v^2}$ - f model in N3S is the backstep flow at $Re = 5,100$, for which the DNS data of Le *et al.* (1993) are available. The simulation with N3S is validated by comparison against results (Durbin, 1995) given by the finite difference code INS2D developed at the NASA Ames Research Center.

A symmetry boundary condition is applied since the calculation domain used for this configuration is symmetric (double backstep). DNS profiles are

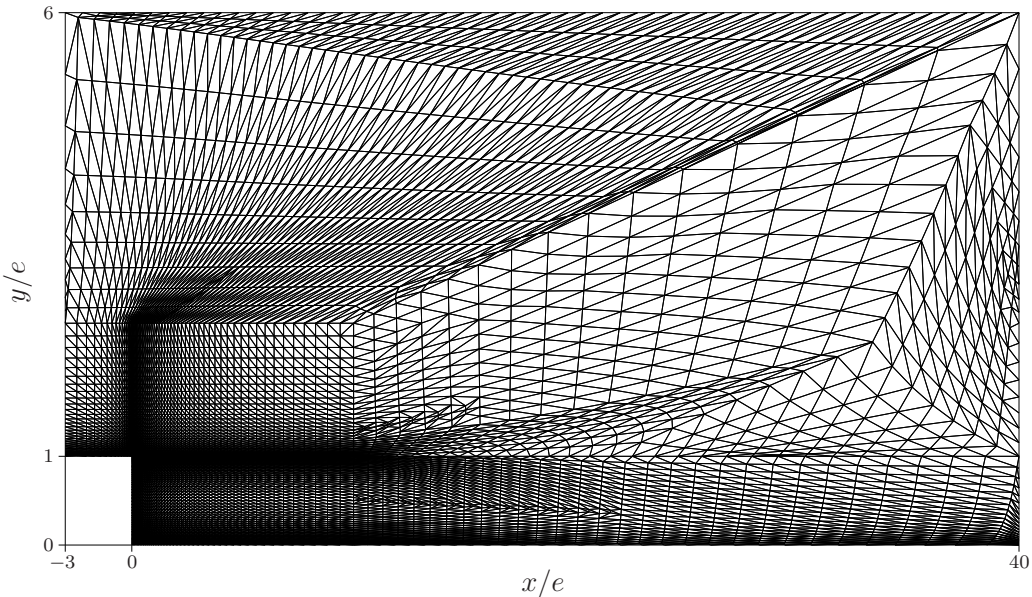


Figure 4: P1 mesh used for the backstep flow.

imposed at the inlet for all the transported variables, including $\overline{v^2}$, which is equal to the wall-normal Reynolds stress in this portion of channel. Regarding f , the Neumann boundary condition $\partial f / \partial \mathbf{n} = 0$ is applied at the inlet, \mathbf{n} denoting the unit vector normal to the inlet plane.

The P1 mesh is shown in Fig. 4. It contains 6,229 nodes, which corresponds to 24,637 P2 nodes. Similarly to the channel flow, the mesh has been chosen excessively fine in order to avoid numerical errors.

The results obtained for the streamwise mean velocity are shown in Fig. 5. Again, a quasi-perfect coincidence between the profiles given by N3S and those given by the reference code can be observed, in spite of the different meshes and numerical techniques. This result achieves the validation of the implementation. However, a slight discrepancy appears in Fig. 6 in which the friction coefficient C_f is plotted: it probably comes from the *a posteriori* evaluation of the velocity derivative at the wall on different meshes and not from the different numerical methods. The mesh used here is actually highly non-uniform and demonstrates the robustness of the current $\overline{v^2}$ - f implementation.

By comparison with the DNS, it can be seen that the predictions of the $\overline{v^2}$ - f model are very satisfactory in this case. Even if the turbulence intensity is slightly overestimated in the recirculation bubble and underestimated above it (not shown here), the velocity profiles are in excellent agreement with DNS data. The main characteristics of this flow, which turbulence mod-

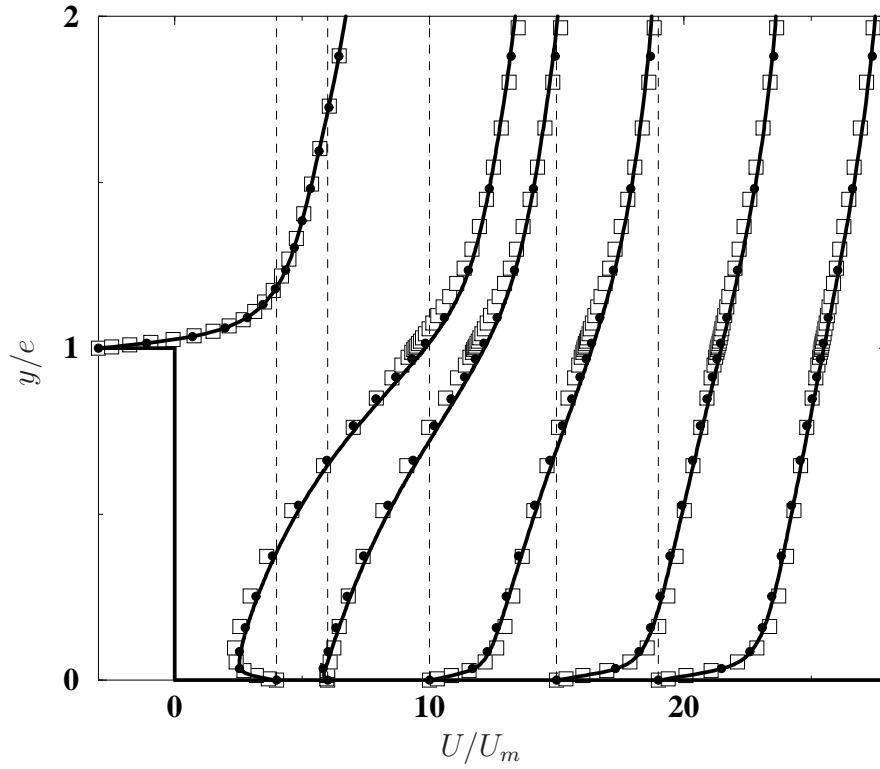


Figure 5: Validation of the implementation in N3S. Backward-facing step at $Re = 5, 100$. Mean velocity profiles. • NASA code; — N3S; □ DNS (Le *et al.*, 1993).

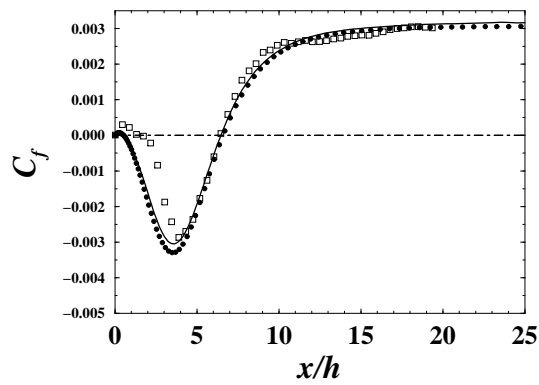


Figure 6: Validation of the implementation in N3S. Backward-facing step at $Re = 5, 100$. Friction coefficient on the lower wall. See Fig. 5 for legend.

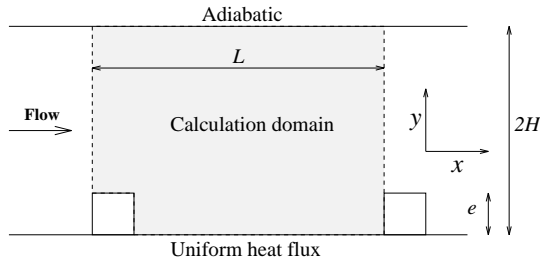


Figure 7: Ribbed-channel flow. Geometry of the test case ($2H=5e$; $L=7.2e$).

els generally fail to predict simultaneously, namely the recirculation length, the back-flow intensity and the recovery of the boundary layer, are correctly reproduced here.

The correct predictions of the back-flow intensity and the friction coefficient is a very interesting result in the frame of nuclear engineering. Indeed, the accurate reproduction of the near-wall region leads to the hope of quantitative accurate predictions of heat transfer between the fluid and the wall.

In the next section, a case more relevant for industrial applications (turbine cooling, for instance) will be investigated: the case of a channel in which ribs are periodically mounted on one wall in order to enhance heat transfer.

4 Test case: periodic ribbed-channel

The geometry of the problem is shown in Fig. 7. Two sets of experimental data have been selected: the first one, from Drain and Martin (1985), containing only velocity measurements, corresponds to the Reynolds number $Re_H = 37,200$, based on the bulk velocity and the hydraulic diameter; the second one, from Liou *et al.* (1993), with temperature measurements at $Re_H = 12,600$. Two different simulations have been performed on the same mesh, shown in Fig. 8, containing 11,548 P1 nodes and 45,738 P2 nodes. Periodic boundary conditions are applied, since only the fully-developed flow is considered here.

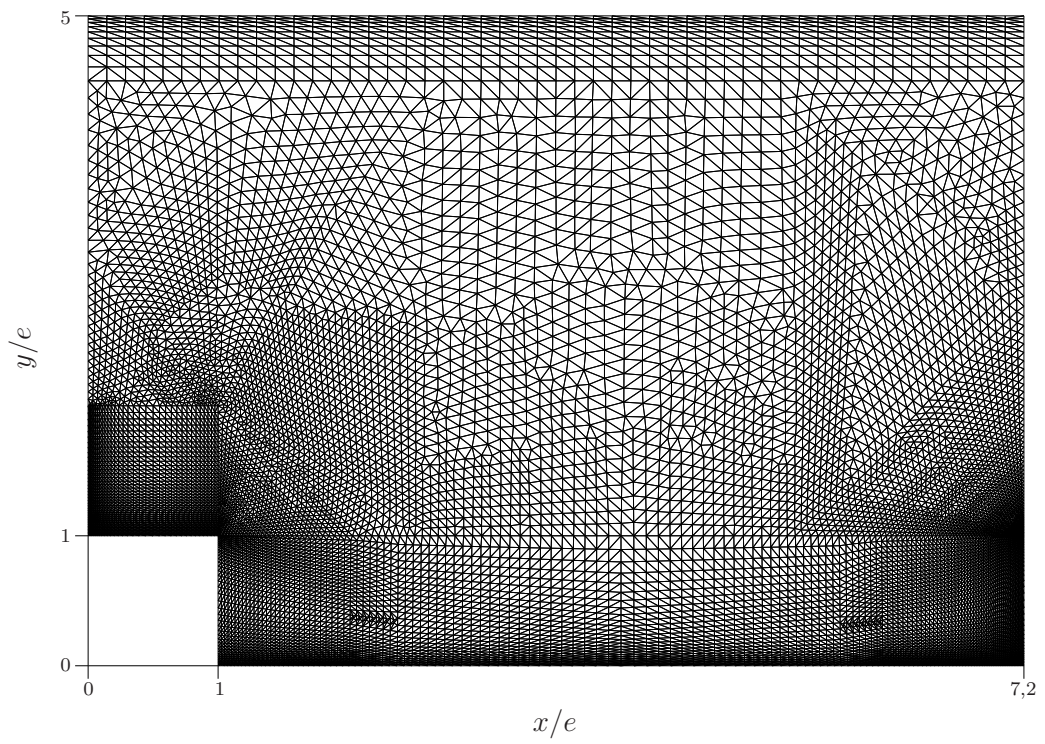


Figure 8: P1 mesh used for the ribbed-channel flow.

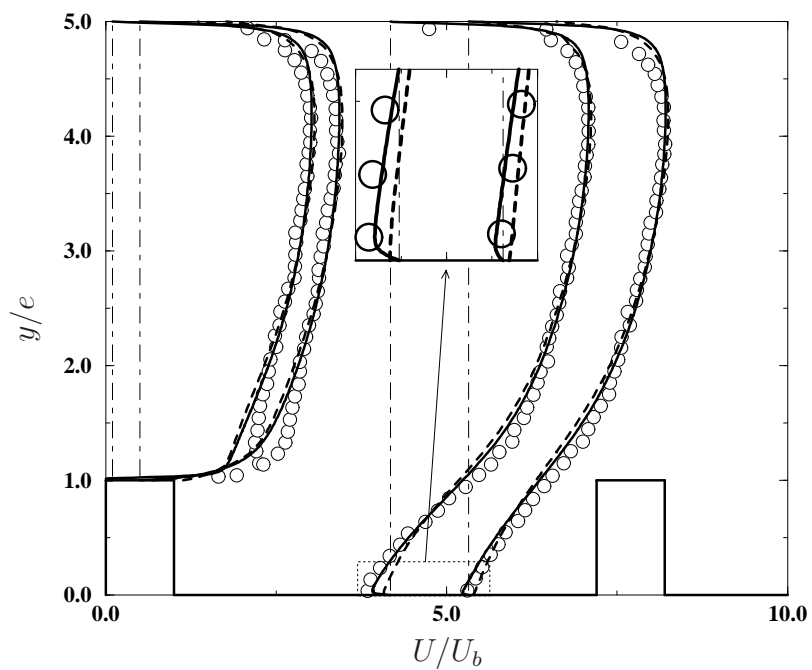


Figure 9: Ribbed-channel flow at $Re_H = 37,200$. Mean streamwise velocity U . \circ Experiments (Drain and Martin, 1985); $—$ $\overline{v^2-f}$ model; $- - -$ Standard $k-\varepsilon$ model with wall functions.

4.1 Case at $Re_H = 37,200$ without heat transfer

Only U , $\overline{u^2}$, $\overline{v^2}$ and \overline{uv} are available in the database. Accordingly, the only variable of the model that can be directly compared with the experiments is the mean streamwise velocity U , which is plotted in Fig. 9. Results obtained with the standard k - ε model with wall functions are also shown. Note that the mesh used for the latter simulation (not shown here) is significantly coarser than that shown in Fig. 8 in order to comply with the y^+ requirements.

It can be seen that the velocity profiles given by the $\overline{v^2}$ - f and the k - ε models are very similar in the main part of the flow, except in the recirculation bubble. Actually, in the rest of the domain, the flow is mainly determined by the geometry induced pressure field. Turbulence plays a significant role only in the recirculation bubble and in the shear layer between the latter and the rest of the flow.

Compared with experiments, both models seems to slightly overpredict the velocity in the upper part of the channel, and to underpredict it in the region just above the ribs, located approximately between $y/e = 1$ and $y/e = 2$. However, this is a feature common to all the results obtained with different models and presented by different teams, using different codes at the seventh ERCOFTAC/IARH workshop on refined turbulence modelling in Manchester (1998). This shows that the experiments probably exhibit 3D effects: counter rotating eddies in the x -direction located between the top of the ribs and the upper wall of the channel can indeed induce an acceleration of the flow in the measurement plane where they converge and a deceleration where they diverge. It is thus dangerous to draw any conclusion about the performance of the model in this flow region.

Close to the lower wall between two consecutive ribs, it can be seen that the $\overline{v^2}$ - f model, correctly reproduces the intensity of the back-flow, even if a slight underestimation is observed. At the location $x/e = 5.32$, the experiments exhibit a very weak back-flow, which shows that there is probably no reattachment: the two recirculation bubbles, after one rib and before the next one, may be actually connected. This feature has been confirmed by a Large Eddy Simulation performed at EDF and also presented at the workshop. The merging of the two bubbles is observed in Fig. 10, in which the streamlines obtained with the $\overline{v^2}$ - f model are plotted. As far as the k - ε model is concerned, it predicts too small separated bubbles and a much too weak back-flow. This result is consistent with the standard behaviour of this type of turbulence model in such separated flows.

Since the $\overline{v^2}$ - f model uses the turbulent viscosity concept, it is interesting to compare against experiments the shear stress obtained by the Boussinesq

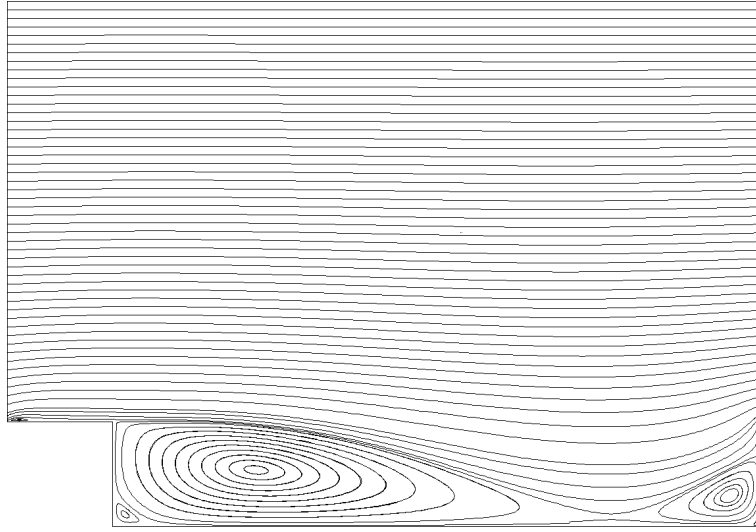


Figure 10: Streamlines obtained with the $\overline{v^2}$ - f model. Ribbed-channel flow at $Re_H = 37,200$.

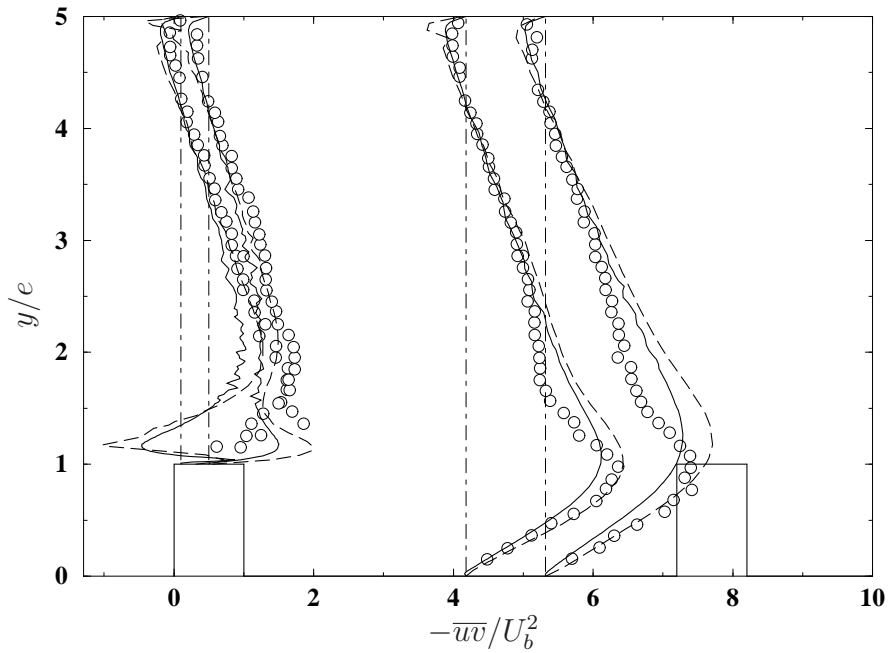


Figure 11: Ribbed-channel flow at $Re_H = 37,200$. Shear stress given by the Boussinesq equation. Irregularities are not due to numerical problems but to the post-processing (velocity gradients calculations on an unstructured mesh). \circ Experiments (Drain & Martin, 1985); — $\overline{v^2}$ - f model; ---- Standard k - ϵ model with wall functions.

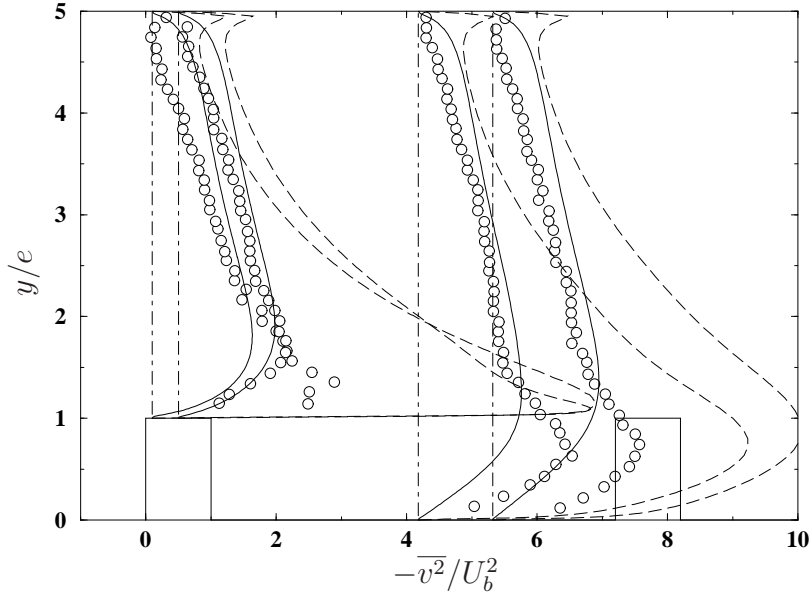


Figure 12: Ribbed-channel flow at $Re_H = 37,200$. Comparison between the $\overline{v^2}$ of the model and the Reynolds stress component $\overline{u_2 u_2}$. \circ Experimental $\overline{u_2 u_2}$ (Drain & Martin, 1985); — $\overline{v^2}$ from the $\overline{v^2}$ - f model; - - - Reynolds stress $\overline{u_2 u_2}$ given by the Boussinesq equation.

approximation. The $-\overline{uv}$ profiles are shown in Fig. 11. With the $\overline{v^2}$ - f model, as well as with the k - ε model, the prediction by the Boussinesq equation is very far from the experiments just above the rib, in particular at $x/e = 0.1$. The profiles at the locations $x/e = 4.18$ and $x/e = 5.32$ are globally correctly reproduced, but the discrepancy remains significant, for both models, between $y/e = 1$ and $y/e = 2.5$.

The $\overline{v^2}$ - f model also contains a transport equation for a scalar velocity scale $\overline{v^2}$ which gives an indication of the anisotropy. Even if this $\overline{v^2}$ and the Reynolds stress component $\overline{u_2 u_2}$ are strictly similar only in the case of the channel flow, it can be interesting to compare them in the present case. It is observed in Fig. 12 that the $\overline{v^2}$ of the model is rather close to $\overline{u_2 u_2}$ in the upper part of the domain, where the flow is similar to a channel flow. In the recirculation bubble, the two quantities are quite different. However, it can be seen that the $\overline{v^2}$ of the model gives a good estimate of the anisotropy, contrary to the Reynolds stress $\overline{u_2 u_2}$ evaluated by the Boussinesq equation, also plotted in the figure. This shows that $\overline{v^2}$ is a much better estimator of near-wall turbulence transport levels than k .

The lack of experimental data and the doubt about the perfectly 2D

character of the experiment do not allow to draw definitive conclusions about this case. However, the correct prediction of the intensity of the back-flow is encouraging for the following heat transfer case.

4.2 Heat transfer case at $Re_H = 12,600$

In this case, a constant heat flux \dot{q}_w is imposed at the lower wall (cf. Fig. 7). The Nusselt number is available from the experiments by Liou *et al.* (1993). It is defined by

$$Nu = \frac{\dot{q}_w D_e}{\lambda(\Theta_w - \Theta_b)} \quad (21)$$

where D_e is the hydraulic diameter, λ the thermal conductivity, Θ_w the mean temperature at the wall and Θ_b the bulk temperature defined by

$$\Theta_b = \int_0^{2h} \Theta |U| y \, dy / \int_0^{2h} |U| y \, dy \quad (22)$$

The temperature being considered as a passive quantity, its calculation and that of the dynamic field are uncoupled. First, the velocity field is evaluated at $Re_H = 12,600$ and secondly, the energy equation is solved with a frozen velocity field.

In the latter simulation, two different types of boundary conditions can be applied. The first one consists in coupling the fluid problem with the conduction problem in the rib. The second one consists in considering that the constant heat flux imposed at the lower face of the rib is equally distributed on the other faces. The first solution is closer to the physics, but more difficult to apply; the second one is simpler, allowing the use of a constant heat flux $\dot{q}_w/3$ on the rib faces. The first solution has been chosen in order to respect as much as possible the experimental conditions. The coupling between the Syrthes code, also developed at EDF, and N3S, enables the resolution of fluid–solid heat transfer problems. However, in order to investigate the influence of the boundary conditions in this case, a simulation with the constant heat flux $\dot{q}_w/3$ at the rib faces has also been performed.

The thermal field is obtained by solving the transport equation of the mean temperature Θ :

$$\frac{D\Theta}{Dt} = \alpha \frac{\partial^2 \Theta}{\partial x_k \partial x_k} - \frac{\partial \overline{u_k \theta}}{\partial x_k} \quad (23)$$

where θ is the fluctuating temperature and α the thermal diffusivity. The thermal fluxes are simply modelled by a turbulent diffusivity hypothesis:

$$\overline{u_k \theta} = -\alpha_T \frac{\partial \Theta}{\partial x_k} \quad (24)$$

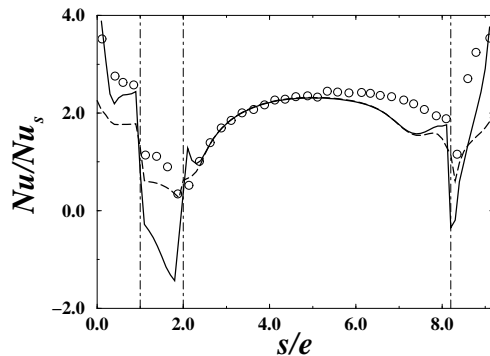


Figure 13: Ribbed-channel flow at $Re_H = 12,600$. Heat transfer enhancement. s is the curvilinear coordinate. $s = 0$ corresponds to the upstream upper corner of the rib. \circ Experiments (Liou *et al.*, 1993); — Computation with coupled fluid–solid heat transfer resolution; ---- Computation with imposed flux on the rib faces.

where the turbulent diffusivity α_T is expressed as a function of the eddy viscosity:

$$\alpha_T = \frac{\nu_T}{Pr_T} \quad (25)$$

The turbulent Prandtl number Pr_T is given by the Kays and Crawford (1993) correlation

$$Pr_T = \frac{1}{0.5882 + 0.228(\nu_T/\nu) - 0.0441(\nu_T/\nu)^2 [1 - \exp(-5.165/(\nu_T/\nu))]} \quad (26)$$

This correlation has been derived in order to fit the variations of Pr_T from about 1.2 at the wall to 0.85 far from it, and provide reasonable values in most of the applications.

The predicted Nusselt number Nu is shown in Fig. 13, normalised by Nu_s , the Nusselt number for the turbulent flow in a smooth circular pipe, given by the Dittus–Boelter correlation:

$$Nu_s = 0.023 Re^{0.8} Pr^{0.4} \quad (27)$$

where Pr is the molecular Prandtl number of the fluid. The ratio Nu/Nu_s characterizes the heat transfer enhancement due to the ribs.

It is observed in Fig. 13 that the Nusselt number distributions obtained with the two different types of boundary conditions are identical, except on the rib faces and in the vicinity of the lower corners of the rib. This shows that the boundary conditions on the rib do not significantly influence the

heat transfer on the main part of the wall. The accuracy of the results is thus not only due to the accounting for the heat conduction in the rib, but also to the turbulence model.

On the rib faces, the results are very different from the experiments. However, on these faces, the heat flux is not known and it is not clear in the paper how the Nusselt number has been evaluated. Again, no definitive conclusions can be drawn as regards the heat flux through these faces.

At the lower wall of the channel, between two consecutive ribs, two parts can be distinguished: the first one, between $s/e = 2$ and $s/e = 5$, where Nu is predicted with an excellent accuracy (less than 5% error locally); the second one, between $s/e = 5$ and $s/e = 8$, where Nu is underestimated (up to 30% error). However, the accuracy of the results is very satisfactory, taking into account the simplicity and robustness of the dynamic and heat transfer models. The average heat transfer level along the ribbed wall, one of the most important parameters for design, is actually quite accurately predicted (about 10% error, certainly below the measurement uncertainty).

The results obtained with the fluid–solid coupled simulation exhibits a negative Nusselt number on the main part of the downstream face of the rib. It comes from the fact that the upstream upper corner is cooled by the flow, whereas the heat accumulates in the vicinity of the downstream lower corner due to the very low velocities in this region. There is then a flux in the rib which transports the heat from the downstream lower corner to the upstream upper corner (see Fig. 14).

5 Conclusion

The possibility of implementing the $\overline{v^2-f}$ model in an industrial code based on a finite element discretization and using unstructured meshes has been demonstrated. Moreover, the ability of the model to reproduce the turbulence characteristics in a case of industrial interest, and, in particular, the heat transfer coefficient, has been shown.

First, the validation cases, the channel and backstep flows, have confirmed that with sufficiently fine meshes, the $\overline{v^2-f}$ results do not depend on the code, even if the numerical methods are completely different, which is not always the case for all turbulence models. The questionable point, i.e. the finite difference approximation to handle the coupled boundary conditions has been proved to be totally successful.

The test case of the ribbed-channel has demonstrated that the $\overline{v^2-f}$ model is a good compromise between the simplicity needed to reduce the cost of the simulations and the accuracy required to reproduce the physical processes,

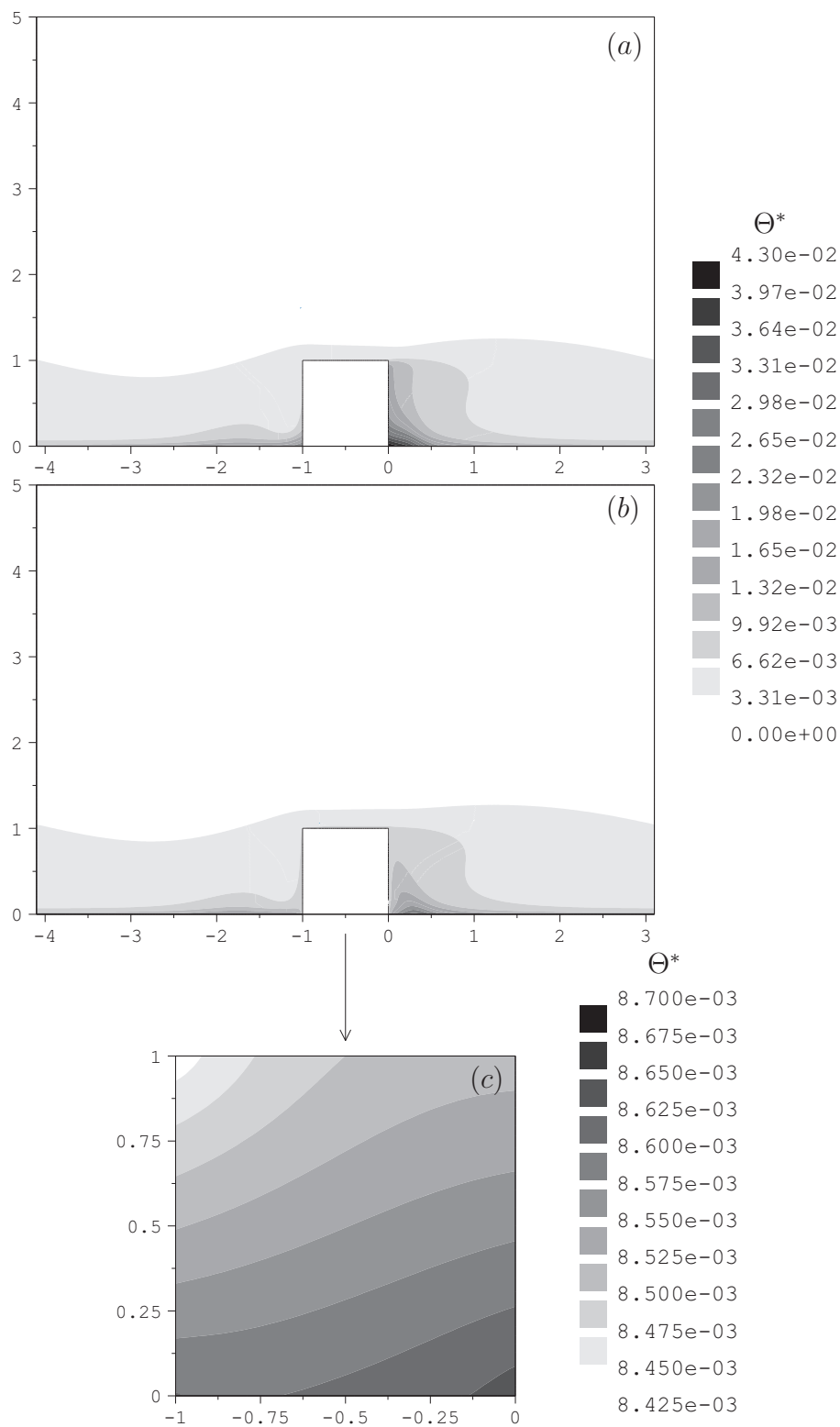


Figure 14: Ribbed-channel flow at $Re_H = 12,600$. Dimensionless mean temperature $\Theta^* = \lambda(\Theta - \Theta_0)/(\dot{q}_w D_e)$, where Θ_0 is the temperature at the adiabatic wall. (a) Computation with imposed flux on the rib faces; (b)–(c) Computation with coupled fluid-solid heat transfer resolution: (b) thermal field in the fluid, (c) thermal field in the rib.

especially the near-wall turbulence anisotropy, decisive for quantitative accuracy in heat transfer predictions. It appears that a very simple model for the heat fluxes is sufficient to successfully predict the Nusselt number distribution, which shows that it is mainly important to use a model that correctly reproduces the dynamic field, especially the turbulence transport levels near solid walls.

The success of the implementation of the $\overline{v^2}$ - f model in a code using unstructured meshes and its ability to predict heat transfer are of primary importance in the context of nuclear engineering. Indeed, it suggests that the model is suitable to “real life” application, in complex geometries, in which the Nusselt number is often the most important quantity to estimate.

References

- Behnia, M., Parneix, S., Durbin, P., 1998. Prediction of heat transfer in a jet impinging on a flat plate, *Intl J. Heat Mass Transfer*, 41, 1845–1855.
- Behnia, M., Parneix, S., Shabany, Y., Durbin, P. A., 1999. Numerical study of turbulent heat transfer in confined and unconfined impinging jets. *Intl J. Heat and Fluid Flow*, 20(1), 1–9.
- Chabard, J. P., Nitrosso, B., Pot, G., 1996. Projet N3S de mécanique des fluides, manuel théorique des versions 3 et 4. Électricité de France, HE-41/96/024/B.
- Craft, T.J., Launder, B.E., Suga, K., 1996. Development and application of a cubic eddy-viscosity model of turbulence. *Intl J. Heat and Fluid Flow*, 17, 108–115.
- Drain, L.E., Martin, S., 1985. Two-component velocity measurements of turbulent flow in a ribbed-wall flow channel. *Intl Conf. Laser Anemometry-Advances and Applications*, 99-112.
- Durbin, P., A., 1991. Near-wall turbulence closure modeling without “damping functions”. *Theoret. Comput. Fluid Dynamics*, 3, 1–13.
- Durbin, P., A., 1995. Separated flow computations with the $k-\varepsilon-\overline{v^2}$ model. *AIAA J.*, 33, 659–664.
- Iacovides, H, Raisee, M., 1999. Recent progress in the computation of flow and heat transfer in internal cooling passages of turbine blades. *Intl J. Heat and Fluid Flow*, 20(3), 320–328.
- Kays, W. M., Crawford, M. E., 1993. *Convective heat and mass transfer*. Third Edition, McGraw-Hill.
- Launder, B. E., 1988. On the computation of convective heat transfer in complex turbulent flows. *J. Heat Transfer*, 110, 1112-1128.
- Le, H., Moin, P., Kim, J., 1993. Direct numerical simulation of turbulent flow over a backward-facing step. *Proc. 9th Symp. Turb. Shear Flows*, 13(2), 1–6.
- Lien, F.-S., Durbin, P., A., Parneix, S., 1997. Non-linear $\overline{v^2} - f$ modelling with application to aerodynamic flows. *Proc. 11th Symp. Turb. Shear Flows*, 6, 19–24.
- Liou, T.-M., Hwang, J.-J., Chen, S.-H., 1993. Simulation and measurement of enhanced turbulent heat transfer in a channel with periodic ribs on one principal wall. *Intl J. Heat Mass Transfer*, 36(2), 507-517.

- Manceau, R., 1999. Modélisation de la turbulence. Prise en compte de l'influence des parois par relaxation elliptique. PhD Dissertation, École centrale de Nantes.
- Manceau, R., Wang, M., Laurence, D., 2000. Inhomogeneity and anisotropy effects on the redistribution term in RANS modelling. Submitted to J. Fluid Mech.
- Moser, R. D., Kim, J., Mansour, N. N., 1999. Direct numerical simulation of turbulent channel flow up to $Re_\tau = 590$. *Phys. Fluids*, 11(4), 943–945.
- Naot, D., Shavit, A. , Wolfshtein, M., 1973. Two-point correlation model and the redistribution of Reynolds stresses. *Phys. Fluids*, 16, 738–743.
- Parneix, S., Behnia, M., Durbin, P., 1998a. Predictions of turbulent heat transfer in an axisymmetric jet impinging on a heated pedestal. *J. Heat Transfer*, 120, 1–7.
- Parneix, S., Durbin, P. A., Behnia, M., 1998b. Computation of 3-D turbulent boundary layers using V2F model. *Flow, Turb. and Comb. J.*, 60(1), 19–46.
- Proceedings of the seventh ERCOFTAC/IARH workshop on refined turbulence modelling, UMIST, Manchester, UK, 28/29th May 1998.
- Van der Worst, H.A., 1992. BI-CGSTAB: A fast and smoothly converging variant of BI-CG for the solution of nonsymmetric linear systems. *SIAM J. Sci. Stat. Comput.*, 13, 631–644.